Euphorbia hirta compound inhibits SARS-CoV-2 main protease: in silico molecular docking and ADME studies

Rasheed-Jada, Hadiza[1]*; Ojochenemi, Enejoh[1]; Okpalefe Okiemute[1].
1National Biotechnology Development Agency (NABDA), Abuja, Nigeria.

Corresponding Author: Phone Number: +2347035602535 Email: hadizamr@gmail.com

Abstract

The COVID-19 pandemic caused by the SARS-CoV-2 virus is responsible for a myriad of deaths globally. There is currently no cure for it, and clinical trials are still on-going for vaccine production. Medicinal plants with good antiviral properties may serve as alternative treatment for COVID-19. The main protease (Mpro) has become an attractive drug target against SARS-CoV-2 in many pieces of research for the development of COVID-19 drugs, and with the absence of closely related human proteases having protease inhibitors that are unlikely to be harmful due to their similar cleavage specificity. Euphorbia hirta has been reported to exhibit antiviral activity. The inhibition of the proteolytic activity of SARS-CoV-2 Mpro by bioactive constituents in Euphorbia hirta may disrupt viral replication. In light of this, the current study investigated inhibition of SARS-CoV-2 Mpro by compounds found in Euphorbia hirta. Secondary metabolites from the plant were mined and molecular docking protocols, using Schrödinger Suite was used to evaluate the compounds for best inhibition properties using Remdesivir as standard. Docking results revealed that ellagic acid (EA) had higher binding affinity -8.608 kcal/mol, compared to Remdesivir (-7.739 kcal/mol). EA also made contact with important amino acids in the active site of the protein via hydrogen bonding. ADME properties of EA were within acceptable ranges, and none of Lipinski's rules were violated. In conclusion, EA could be a potential drug candidate for combating the COVID-19 pandemic by targeting the SARS-CoV-2 Mpro

Keywords: COVID-19, Protein, Replication, Ribonucleic acid, Secondary metabolites, Viral genome.

Introduction

The process of replication is crucial to viral pathogenicity. It is in charge of creating multiple copies of the viral DNA and the proteins that come together to produce new viruses. The novel severe acute respiratory disease coronavirus 2 is responsible for the coronavirus disease 2019 (COVID-19), a pneumonia-like condition (N-SARS-CoV-2), matures as a result of a complicated series of proteolytic processes triggered by polyproteins that control viral gene expression and replication. Enzymes that catalyze expression and replication processes serve as prospective targets for the discovery of antiviral drugs. A coronavirus (CoV) strain known as SARS-CoV-2 is an enclosed, positive-sense, single-stranded RNA virus. A replicase gene in the SARS-CoV-2 genome produces the overlapping polyproteins pp1a and pp1b. During maturation, the major protease (Mpro), a 33.8 kDa cysteine protease, and 3-chymotrypsin-like peptidase (3CLPro) break the nascent polyproteins (Wu et al., 2020). Before activating the subsequent maturation cleavage of replicase polyproteins, Mpro first undergoes self-maturation through autolytic cleavage (Ziebuhr, Snijder, & Gorbalenya, 2000). MPro works in conjunction with another protease, the papain-like protease, to carry out its proteolytic cleavage, cleaving no fewer than 11 cleavage sites of the two overlapping polyproteins (Zhang et al., 2020). It processes from the C-terminus of non-structural proteins (nsps) 4 through 16 (Anand, Ziebuhr, Wadhwani, Mesters, & Hilgenfeld, 2003; Bost, Carnahan, Lu, & Denison, 2000; Denison, Sims, Gibson, & Lu, 1998; Denison et al., 1999; Lu, Sims, & Denison, 1998; Tan et al., 2005); while papain-like protease processes nsps 1 through 3 (Harcourt et al., 2004). The most common recognition sequence at sites is Leu-Gln (Ser, Ala, Gly) (marks the cleavage site), with glutamine almost always required at a specific substrate site (Zhang et al., 2020).Ppa1 and pp1ab are encoded in the first open reading frame (ORF1a/b) and are cleaved into 16 non-structural proteins (nsps 1–16) (Dai et al., 2020). CoV Mpro contains 306 amino acids, and it is nsp 5 of the polyprotein, located in residues 3264–3569 (Mirza & Froeyen, 2020). SARS-CoV replicase gene proteins play pivotal roles in virulence, viral–cell interactions, and alterations of the virus-host immune response (Graham, Sparks, Eckerle, Sims, & Denison, 2008). Three domains (I to III) make up a CoV Mpro protomer, with a two-domain fold at the N-terminus resembling chymotrypsin (Gorbalenya, Koonin, Donchenko, & Blinov, 1989; Lee et al., 1991; Schneider & Sheldrick, 2002). Domain III is composed of five -helices grouped in a substantially antiparallel globular cluster arrangement and connected to domain II by a lengthy loop area. Domains I and II are antiparallel -barrel structures (Jin et al., 2020). The substrate-binding site and a Cys-His dyad are situated in a gap between domains I and II (Anand et al., 2002; Anand et al., 2003; Yang et al., 2003). All CoV MPros have a highly conserved substrate-binding site, which is made up of the following four subsites: S1', S1, S2, and S4 (Yang et al., 2005). While the C-terminus of domain III is reported to be crucial for dimerization primarily through a salt-bridge

contact between Glu290 of one protomer and Arg4 of the other protomer, residues 1–7 of the N-terminus are thought to play a crucial role in the proteolytic activity (Shi & Song, 2006).

Studies have demonstrated that two CoV Mpro molecules can combine to create an active homodimer (Anand et al., 2002; Anand et al., 2003). Since the N-terminus (N-finger) of both protomers interacts with Glu166 of the other protomer to define the shape of the S1 pocket of the substrate-binding site, dimerization of Mpro through various interactions is crucial for its catalytic activity (Anand et al., 2002). With the two molecules oriented perpendicular to one another, the generated SARS-CoV-2 Mpro dimer has a contact interface of 1394 2, primarily between domain II of the first protomer and the N-finger of the second protomer (Zhang et al., 2020). The side-chain hydroxyl group of residue Thr285 in each protomer forms a 2.60 hydrogen bond with the other domain III of the SARS-CoV Mpro dimer to form a polar contact (Zhang et al., 2020). A hydrophobic interaction between the side chains of Ile286 and Thr285 C2 supports this (Zhang et al., 2020). Thr285 and Ile286 are changed to Ala and Leu in the SARS-CoV-2 Mpro dimer, respectively. It is claimed that the Thr285Ala substitution in the SARS-CoV-2 Mpro will boost contact between the two domains III (Zhang et al., 2020).

SARS-CoV-2 Mpro and SARS-CoV have identical three-dimensional structures due to their 96% sequence match (Zhang et al., 2020). Additionally, it shows similarities to the Mpro of other coronaviruses, such as the infectious bronchitis virus (IBV) and transmissible gastroenteritis virus (CoV) (TGEV). By superimposing several co-crystallized SARS-CoV Mpro structures bound with inhibitors N1 (1WOF), I2 (2D2D), and N3 (2AMQ), it has been possible to clarify the similar positioning of the S1, S2, and S4 subsites, particularly in the active site that is close to His41 and Cys145, which are crucial for substrate recognition (Yang et al., 2005), as well as Tyr161 and His163 in the substrate-binding pocket (2AMQ) (Chang, Chou, & Chang, 2007). The SARS-CoV-2 Mpro structural analysis report showed that it shares the same active site with SARS-CoV Mpro, which is located in the cleft between domain I and domain II. These domains each add one residue (His41 and Cys145) to the catalytic dyad (Mirza & Froeyen, 2020). These papers have shed light on how to comprehend the SARS-CoV-2 Mpro active site for drug discovery.

Several studies are now being conducted to find effective medication compounds to treat COVID-19. Remdesivir is the only medication currently licensed by the FDA for the treatment of COVID-19. Worldwide death figures are still being kept track of, though. Respiratory distress and organ dysfunction are negative effects of remdesivir. Since they have less side effects, are less expensive, have higher bioavailability, are abundant in nature, and are a rich source of bioactive ingredients with a lower potential for resistance, medicinal plants have been utilized locally for decades to treat viral illnesses (Mukherjee, Kumar, & Houghton, 2007). They might result in the development of brand-new, very effective inhibitory drugs, which might be employed as a method to tackle COVID-19. The traditional use of Euphorbia hirta includes the treatment of dengue fever, bronchitis, asthma, cough, etc. Direct antiviral or inhibitory activity on HIV-1, HIV-2, and SIV (mac251) reverse transcriptase has been demonstrated for aqueous extracts of E. hirta (Gyuris et al., 2009). In numerous studies for COVID-19 medications, Mpro has emerged as a promising target against SARS-CoV-2, and since there are no closely analogous human proteases with a similar cleavage selectivity, inhibitors against the protease are unlikely to be hazardous (Zhang et al., 2020). Viral replication may be hampered by Bioactive compounds in Euphorbia hirta that hinder the proteolytic activity of SARS-CoV-2 Mpro. In order to target SARS-CoV-2 Mpro, this study aims to evaluate the structure-based inhibitory activity of a few compounds discovered in Euphorbia hirta.

Table 1: displaying the outcomes of a compound's molecular docking with a molecular target

Compounds	Docking rating (kcal/mol)
Co-ligand (11b)	-7.887
Remdesivir	-7.379
Ellagic acid	-8.608

Table 2: ADME properties of compounds employing Qikprop

Compounds	SASA	donorHB	accept	QPlogPo/w	QPlogS	QPlogHERG	QPlogBB	QPPMDCK	QPlogKp	%HOA	ROF
Co-ligand(11b)	850.257	8	12.8	-0.221	0.47	-8.009	-1.477	1.873	-7.619	20.389	1
Remdesivir	790.882	5	16.65	0.942	-3.584	-5.076	-2.749	15.067	-3.856	35.041	

QPlogBB = -3.0-1.2, the predicted blood/brain partition coefficient
Donor of hydrogen bonding, HB donor = 0.0–6.0
Acceptor for hydrogen bonding, HB acceptor = 2.0–20.0
Surface area of all the solvents that are available, SASA = 300.0-1000.0nn
HERG K+ channel blockage predicted IC50 value, QPlogHERG = Concern below -5
Aqueous solubility predicted, QPlogS = -6.5-0.5
O/W partition coefficient predicted, QP log Po/w = -2.0–6.5
Predicted qualitative human oral absorption: strong (>80%), low (25%)
QPPMDCK= >500 is excellent, 25 is low for predicted apparent MDCK cell permeability.
Skin permeability predictions, -8.0 to -10.0 for QPlogKp
The number of violations of Lipinski's rule of five (ROF)

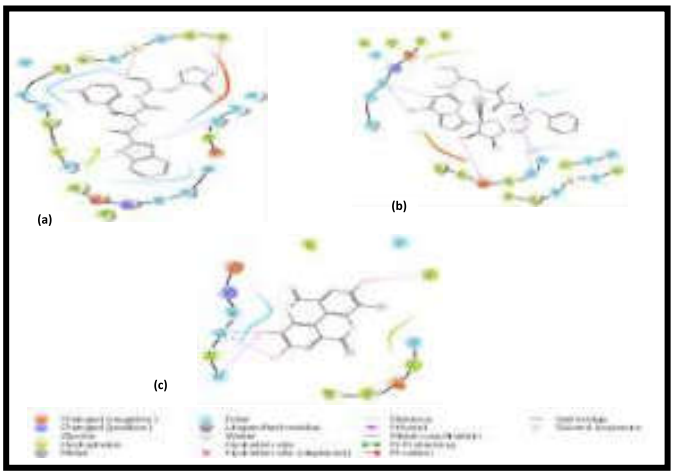

Figure 3:2D interaction view of 11b (a), Remdesivir (b) and Ellagic acid(c), showing hydrogen bonding, pi-pi stacking and

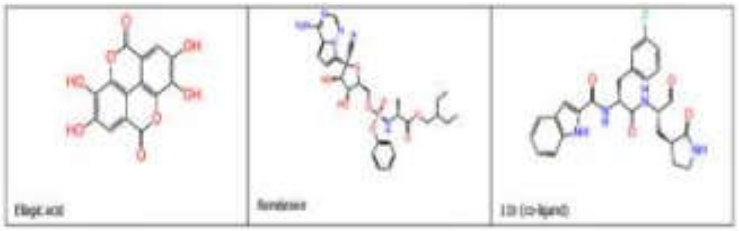

Figure 1: The two-dimensional (2D) structure of compounds .

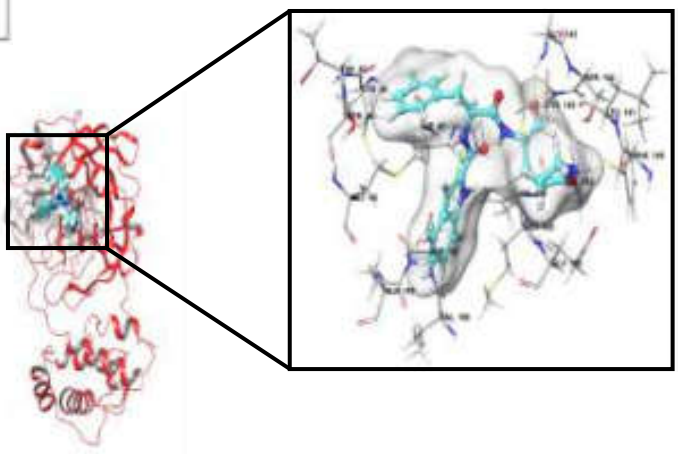

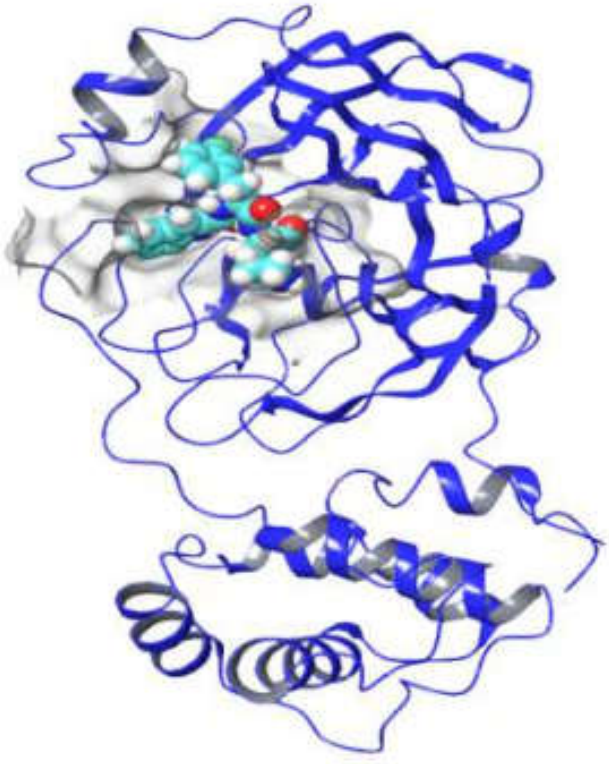

Figure 2: Three dimensional (3D) minimized crystal structure of SARS -CoV-2 main protease

Figure 4: Molecular docking investigation of the Mpro-inhibitor binding mechanism for 11b is represented structurally. SARS-CoV-2 Mpro's crystal structure in complex with 11b as depicted in a cartoon. Wheat sticks are used to illustrate the residues involved in inhibitor binding. The Close-up view of the 11b binding pocket showing the three-dimensional (3D) schematic diagram of SARS-CoV-2 Mpro-11b interactions and the bonding communications are indicated as dashed lines, yellow (H-bond),

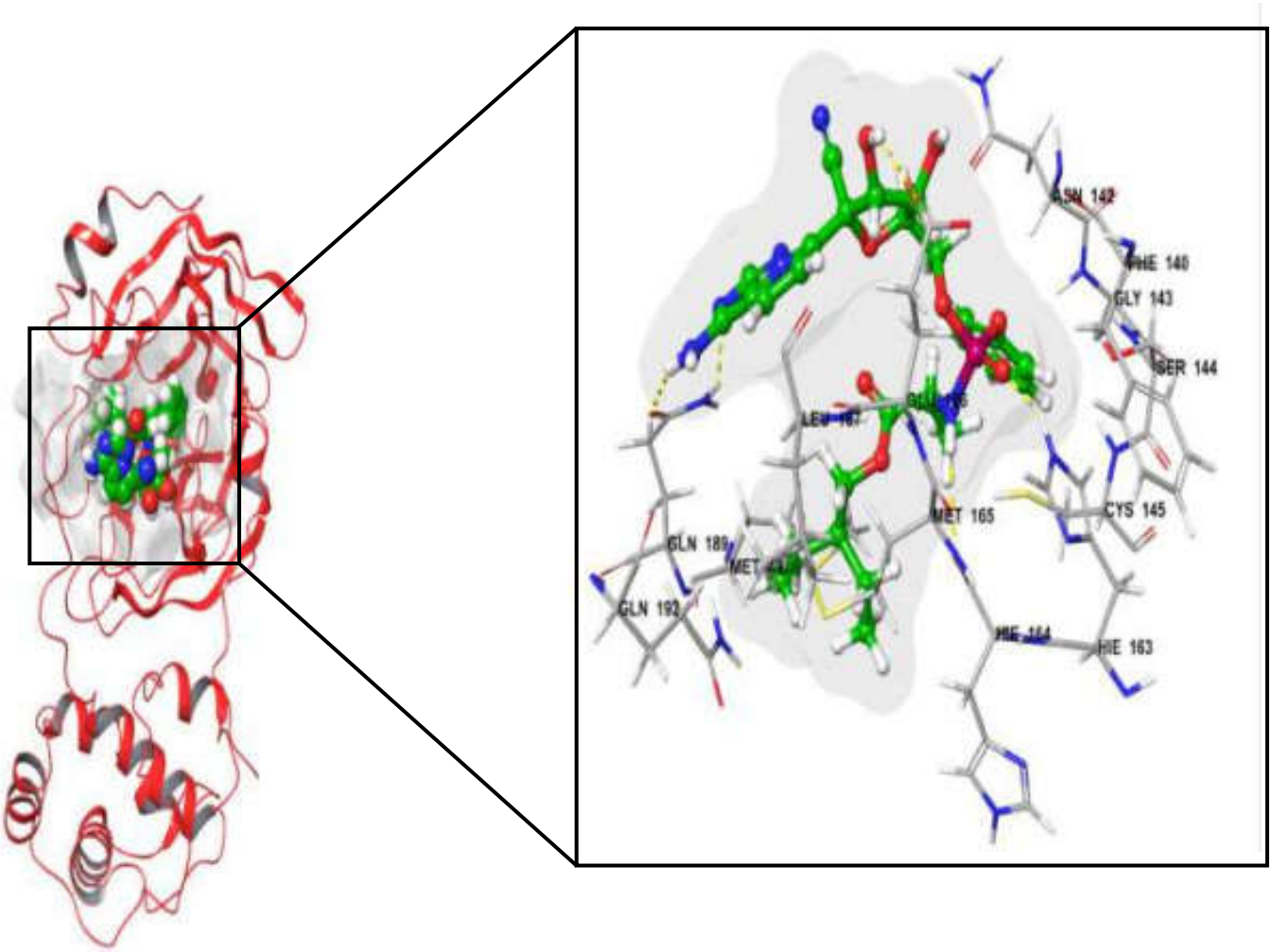

Figure 5: Structure of the Mpro-inhibitor binding mechanism for Remdesivir in a molecular docking investigation. Cartoon representation of the crystal structure of SARS-CoV-2 Mpro in complex with Remdesivir. The residues involved in inhibitor binding are shown as wheat sticks. The Close-up view of the Remdesivir binding pocket showing the three-dimensional (3D) schematic diagram of SARS-CoV-2 Mpro- Remdesivir interactions and the bonding communications are indicate

Material and methods

Protein Preparation

To perform molecular docking analysis, a retrieval of The protein data bank's PBD format was used to create the three-dimensional crystal structure of SARS-CoV-2 Mpro in association with an inhibitor 11b (PDB ID: 6M0K) (Dai et al., 2020). The collected target proteins were tidied and prepared using the Schrödinger-Maestro v11.5.011 Protein Preparation Wizard. Water molecules were removed, charges were allocated, and bond orders were created. The heavier atoms have hydrogens added to them. OPLS3 force field was used to minimize energy while maintaining the heavy atom's RMSD of 0.30. (Shivakumar et al., 2010). A pH of neutral was used to maximize amino acids.

Ligand Preparation

All of the compounds created by E. Hirta (Abu Bakar, Abu Bakar, Abdullah, Endrini, & Fatmawati, 2020) had their 2D structures obtained from the Pubchem database. Ligand preparation was carried out to establish suitable bond ordering and three-dimensional geometries (Sastry, Adzhigirey, Day, Annabhimoju, & Sherman, 2013). OPLS3 force field and Ligprep2.5 from Schrödinger Suite 2018 were used to create three-dimensional geometry. We utilized Epik4.3 in the Schrödinger Suite at pH 7.0 2.0 to create ionization states (Wizard, 2018). There were a maximum of 32 stereoisomers per ligand.

Receptor grid generation

A grid was created around the active site of the produced protein by using the co-crystallized ligand for each target as a guide. Using the OPLS3 force field and a fixed van der Waals scaling factor of 1.0 and charge cut-off value of 0.25, glide docking grids were produced. For docking studies, a box containing 80, 80, 80, and 80 was constructed in each direction..

Extra Precision (XP) ligand docking

For the scoring function, XP ligand docking was done (Friesner et al., 2006). This docking was performed in Glide

of Schrödinger-Maestro v11.5, with the van der Waals scaling factor set at 0.85 and 0.15 for ligand compounds.

Molecular Docking

The current study used virtual screening to identify the protein conformation that is most compatible with the plant ingredients while also narrowing the ligand library to compounds with high affinity and specificity to the target proteins. We noticed that the plant components readily bind to the crystal structure of the SARS-CoV-2 major protease (Mpro) in the inhibitory-bound state (6M0K) depicted in figure 2 with lower G values and higher affinity. This suggests that the phytochemicals in E. hirta have strong inhibitory activity. Although different groups of compounds were found in the plant, we concentrated on all phytochemicals for the current investigation in order to pick the top members for additional molecular interaction profiling and pharmacological examination. The Glide extreme precision (XP) method is a potent docking and scoring function that is more discriminating. Ellagic acid, the lead compound with a higher binding affinity of -8.608 kcal/mol glide docking score against the previously reported standard inhibitor (Remdesivir), and co-crystallized ligand (11b) binding affinities of -7.739 and -7.887kcal/mol glide docking score were found when the E. hirta phytoconstituents were docked to the inhibitory-bound enzyme-protein respectively as shown in table 1 with their two-dimensional structure (2D) shown in figure 2. We examined the XP-glide docked pose of Ellagic acid in comparison to Remdesivir and 11b in order to better understand the binding method of the substance with the best score against those two drugs. Figures 3(a) and 4 illustrate the extended conformational binding mode of protein 11b in the substrate-binding pocket of SARS-CoV-2 Mpro. Details of the interaction are also displayed. According to the investigation, a C-S covalent bond was established between the catalytic site Cys145 of the SARS-CoV-2 Mpro and the aldehyde group of 11b. Through the establishment of a hydrogen bond with the backbone of Cys145, a residue that makes up the S1' site, the oxygen atom of the aldehyde group also plays a significant part in maintaining the conformations of the inhibitor. The P1 site of 11b's (S)—lactam ring easily accommodates the S1 site. The oxygen in the (S)-lactam group creates a hydrogen connection (bond) with the side chain of His163. Both the side chain of Glu166 and the main chain of Phe140 help to stabilize the (S)—lactam ring by forming a hydrogen bond with their respective NH groups. Additionally, His163 and His164's major chains form hydrogen connections with the amide bonds on the chain of 11b. In the S2 site, the cyclohexyl moiety of 11b at P2 pi-stacks with the imidazole ring of His 41. The side chains of Met49, Tyr25, Met165, Asp187, and Arg188 are also present around the cyclohexyl group, providing a significant amount of hydrophobic support. Glu166 stabilizes the indole group of 11b at P3 which is accessible to solvent (S4 site). Hydrophobic contacts were discovered around the side chains of the residues His41, Met49, Met165, Val186, Asp187, and Arg188 that interact with aryl groups. Our docking method was validated by the fact that this interaction is almost identical to the reported inhibitory modes by Dai et al. (Dai et al., 2020).

Remdesivir's mechanism of binding to the SARS-CoV-2 Mpro is depicted in Figure 5. Remdesivir has broad-spectrum antiviral activity against RNA viruses, according to preliminary reports, and studies with RdRps from the Ebola virus (EBOV), Middle East respiratory syndrome coronavirus (MERS-CoV), and SAR-Cov-2 have shown that delayed chain-termination is Remdesivir's plausible mode of action in vivo (Al-Tawfiq, Al-Homoud, & Memish, 2020; Gordon et al., 2020). We detected some of the binding mode of 11b (figures 4 and 3 (a)) in Remdesivir binding after the analysis from posture was shown in figures 5 and 3 (b) exhibiting the 3D and 2D interactions. The His163 side chain and the phenoxyphosphoryl amino propanoate group form a hydrogen connection at the S1' site. By forming a hydrogen bond with the side chain of Glu166, it also helps to stabilize the 3,4-dihydroxyoxolan-2-yl group. According to Dai et al., the Remdesivir 4-aminopyrrolo structure adopts hydrogen bond communication with Gln189, which makes up the S4 site for stability inside the SARS-CoV-2 Mpro substrate binding site (Dai et al., 2020).
Ellagic acid, the component with the highest score, is in the XP-glide posture. Ellagic acid is an organic heterotetracyclic molecule that is created when Gallic acid is formal dimerized through oxidative aromatic coupling and intramolecular lactonization of both of the ensuing biaryl's carboxylic acid groups. From figure 6 and figure 3 (c), it shows the 3D and 2D interaction of ellagic acid within the SARS-CoV-2 Mpro substrate binding site. We observed that ellagic acid exhibit its inhibitory occupancy by occupying site located in the cleft between domain I and II at the active site of SARS-CoV-2 Mpro and adopt hydrogen bond with Cys145 to stabilize within SARS-CoV-2 Mpro catalytic dyad. The tetrahydroxy group of ellagic acid pack two (2) hydrogen bonding with Thr190 and Gln 192 for stability within the catalytic dyad. Interestingly, a wealth of in vivo (Cui et al., 2018; Park, Kwon, Yoo, Choi, & Ahn, 2014) and in silico experiment has documented antiviral effect of Ellagic acid. This indicates that the ligand was in its most favourable conformations. Hydrogen bonds formed in the catalytic site residues on protein-ligand complex confirms the potent binding and perfect docking on the ligand. This evidences that the Ellagic acid has a good inhibitory activity which possesses potent antiviral activity against SARS-CoV-2 Mpro.

ADME investigation

The characteristics of the compounds are illustrated by their bioavailability, distribution, cell permeability, excretion, and absorption qualities. The ADME qualities of the standard compound (Remdesivir), Co-ligand (11b), and ellagic acid were evaluated to elucidate the pharmacokinetic features.

Table 2 depicts the ADME characteristics of the reference compound (Remdesivir), the co-ligand (11b), and ellagic acid were evaluated to better understand the pharmacokinetic features. Ellagic acid showed QPlogBB value of -2.395, which is within the acceptable range of -3.0-1.2. The ADME properties of the reference compound (Remdesivir), the co-ligand (11b), and ellagic acid were examined to further understand the pharmacokinetic features. Percentage human oral absorption rate is lower in co-ligand, showing a poor value, but Ellagic acid and Remdesvir are within the acceptable range according to the findings of our study.

Conclusion

All compounds were within the acceptable range, which is -2.0 to 6.5. The percentage of human oral absorption rate is lower in co-ligand, showing a poor value, but Ellagic acid and Remdesvir are within the acceptable range according to the findings of this study. In the case of cell permeability, all compounds showed lower values, which is a crucial parameter for a drug to pass through the cell to be active. Skin permeability was very poor compared to the acceptable range of -8.0 to -10.0. The rule of five violations was also observed, Remdesivir and co-ligand showed a level of violations, but Ellagic acid violates none of the rules. Thus, the study portrayed that the best docking and good drug-likeliness profiles were exhibited by Ellagic acid.

References

1. Abu Bakar, F. I., Abu Bakar, M. F., Abdullah, N., Endrini, S., & Fatmawati, S. (2020). Optimization of Extraction Conditions of Phytochemical Compounds and Anti-Gout Activity of Euphorbia hirta L. (Ara Tanah) Using Response Surface Methodology and Liquid Chromatography-Mass Spectrometry (LC-MS) Analysis. Evid Based Complement Alternat Med, 2020, 4501261. https://doi.org/10.1155/2020/4501261
2. Al-Tawfiq, J. A., Al-Homoud, A. H., & Memish, Z. A. (2020, Mar 5). Remdesivir as a possible therapeutic option for the COVID-19. Travel Med Infect Dis, 101615. https://doi.org/10.1016/j.tmaid.2020.101615
3. Anand, K., Palm, G. J., Mesters, J. R., Siddell, S. G., Ziebuhr, J., & Hilgenfeld, R. (2002, Jul 1). Structure of coronavirus main proteinase reveals combination of a chymotrypsin fold with an extra alpha-helical domain. EMBO J, 21(13), 3213-3224. https://doi.org/10.1093/emboj/cdf327
4. Anand, K., Ziebuhr, J., Wadhwani, P., Mesters, J. R., & Hilgenfeld, R. (2003, Jun 13). Coronavirus main proteinase (3CLpro) structure: basis for design of anti-SARS drugs. Science, 300(5626), 1763-1767. https://doi.org/10.1126/science.1085658
5. Bost, A. G., Carnahan, R. H., Lu, X. T., & Denison, M. R. (2000, Apr). Four proteins processed from the replicase gene polyprotein of mouse hepatitis virus colocalize in the cell periphery and adjacent to sites of virion assembly. J Virol, 74(7), 3379-3387. https://doi.org/10.1128/jvi.74.7.3379-3387.2000
6. Chang, H. P., Chou, C. Y., & Chang, G. G. (2007, Feb 15). Reversible unfolding of the severe acute respiratory syndrome coronavirus main protease in guanidinium chloride. Biophys J, 92(4), 1374-1383. https://doi.org/10.1529/biophysj.106.091736
7. Cui, Q., Du, R., Anantpadma, M., Schafer, A., Hou, L., Tian, J., Davey, R. A., Cheng, H., & Rong, L. (2018, Mar 27). Identification of Ellagic Acid from Plant Rhodiola rosea L. as an Anti-Ebola Virus Entry Inhibitor. Viruses, 10(4). https://doi.org/10.3390/v10040152
8. Dai, W., Zhang, B., Su, H., Li, J., Zhao, Y., Xie, X., Jin, Z., Liu, F., Li, C., Li, Y., Bai, F., Wang, H., Cheng, X., Cen, X., Hu, S., Yang, X., Wang, J., Liu, X., Xiao, G., Jiang, H., Rao, Z., Zhang, L. K., Xu, Y., Yang, H., & Liu, H. (2020, Apr 22). Structure-based design of antiviral drug candidates targeting the SARS-CoV-2 main protease. Science. https://doi.org/10.1126/science.abb4489
9. Denison, M. R., Sims, A. C., Gibson, C. A., & Lu, X. T. (1998). Processing of the MHV-A59 gene 1 polyprotein by the 3C-like proteinase. Adv Exp Med Biol, 440, 121-127. https://doi.org/10.1007/978-1-4615-5331-1_16
10. Denison, M. R., Spaan, W. J., van der Meer, Y., Gibson, C. A., Sims, A. C., Prentice, E., & Lu, X. T. (1999, Aug). The putative helicase of the coronavirus mouse hepatitis virus is processed from the replicase gene polyprotein and localizes in complexes that are active in viral RNA synthesis. J Virol, 73(8), 6862-6871. https://www.ncbi.nlm.nih.gov/pubmed/10400784
11. Friesner, R. A., Murphy, R. B., Repasky, M. P., Frye, L. L., Greenwood, J. R., Halgren, T. A., Sanschagrin, P. C., & Mainz, D. T. (2006, Oct 19). Extra precision glide: docking and scoring incorporating a model of hydrophobic enclosure for protein-ligand complexes. J Med Chem, 49(21), 6177-6196. https://doi.org/10.1021/jm051256o
12. Gorbalenya, A. E., Koonin, E. V., Donchenko, A. P., & Blinov, V. M. (1989, Jun 26). Coronavirus genome: prediction of putative functional domains in the non-structural polyprotein by comparative amino acid sequence analysis. Nucleic Acids Res, 17(12), 4847-4861. https://doi.org/10.1093/nar/17.12.4847
13. Gordon, C. J., Tchesnokov, E. P., Woolner, E., Perry, J. K., Feng, J. Y., Porter, D. P., & Gotte, M. (2020, May 15). Remdesivir is a direct-acting antiviral that inhibits RNA-dependent RNA polymerase from severe acute respiratory syndrome coronavirus 2 with high potency. J Biol Chem, 295(20), 6785-6797. https://doi.org/10.1074/jbc.RA120.013679
14. Graham, R. L., Sparks, J. S., Eckerle, L. D., Sims, A. C., & Denison, M. R. (2008, Apr). SARS coronavirus replicase proteins in pathogenesis. Virus Res, 133(1), 88-100. https://doi.org/10.1016/j.virusres.2007.02.017
15. Gyuris, A., Szlavik, L., Minarovits, J., Vasas, A., Molnar, J., & Hohmann, J. (2009, May-Jun). Antiviral activities of extracts of Euphorbia hirta L. against HIV-

1, HIV-2 and SIVmac251. In Vivo, 23(3), 429-432. https://www.ncbi.nlm.nih.gov/pubmed/19454510
16. Harcourt, B. H., Jukneliene, D., Kanjanahaluethai, A., Bechill, J., Severson, K. M., Smith, C. M., Rota, P. A., & Baker, S. C. (2004, Dec). Identification of severe acute respiratory syndrome coronavirus replicase products and characterization of papain-like protease activity. J Virol, 78(24), 13600-13612. https://doi.org/10.1128/JVI.78.24.13600-13612.2004
17. Jin, Z., Du, X., Xu, Y., Deng, Y., Liu, M., Zhao, Y., Zhang, B., Li, X., Zhang, L., Peng, C., Duan, Y., Yu, J., Wang, L., Yang, K., Liu, F., Jiang, R., Yang, X., You, T., Liu, X., Yang, X., Bai, F., Liu, H., Liu, X., Guddat, L. W., Xu, W., Xiao, G., Qin, C., Shi, Z., Jiang, H., Rao, Z., & Yang, H. (2020, Apr 9). Structure of M(pro) from SARS-CoV-2 and discovery of its inhibitors. Nature. https://doi.org/10.1038/s41586-020-2223-y
18. Lee, H. J., Shieh, C. K., Gorbalenya, A. E., Koonin, E. V., La Monica, N., Tuler, J., Bagdzhadzhyan, A., & Lai, M. M. (1991, Feb). The complete sequence (22 kilobases) of murine coronavirus gene 1 encoding the putative proteases and RNA polymerase. Virology, 180(2), 567-582. https://doi.org/10.1016/0042-6822(91)90071-i
19. Lu, X. T., Sims, A. C., & Denison, M. R. (1998, Mar). Mouse hepatitis virus 3C-like protease cleaves a 22-kilodalton protein from the open reading frame 1a polyprotein in virus-infected cells and in vitro. J Virol, 72(3), 2265-2271. https://www.ncbi.nlm.nih.gov/pubmed/9499085
20. Mirza, M. U., & Froeyen, M. (2020, Apr 28). Structural elucidation of SARS-CoV-2 vital proteins: Computational methods reveal potential drug candidates against main protease, Nsp12 polymerase and Nsp13 helicase. J Pharm Anal. https://doi.org/10.1016/j.jpha.2020.04.008
21. Mukherjee, P. K., Kumar, V., & Houghton, P. J. (2007, Dec). Screening of Indian medicinal plants for acetylcholinesterase inhibitory activity. Phytother Res, 21(12), 1142-1145. https://doi.org/10.1002/ptr.2224
22. Park, S. W., Kwon, M. J., Yoo, J. Y., Choi, H. J., & Ahn, Y. J. (2014, May 26). Antiviral activity and possible mode of action of ellagic acid identified in Lagerstroemia speciosa leaves toward human rhinoviruses. BMC Complement Altern Med, 14, 171. https://doi.org/10.1186/1472-6882-14-171
23. Sastry, G. M., Adzhigirey, M., Day, T., Annabhimoju, R., & Sherman, W. (2013, Mar). Protein and ligand preparation: parameters, protocols, and influence on virtual screening enrichments. J Comput Aided Mol Des, 27(3), 221-234. https://doi.org/10.1007/s10822-013-9644-8
24. Schneider, T. R., & Sheldrick, G. M. (2002, Oct). Substructure solution with SHELXD. Acta Crystallogr D Biol Crystallogr, 58(Pt 10 Pt 2), 1772-1779. https://doi.org/10.1107/s0907444902011678
25. Shi, J., & Song, J. (2006, Mar). The catalysis of the SARS 3C-like protease is under extensive regulation by its extra domain. FEBS J, 273(5), 1035-1045. https://doi.org/10.1111/j.1742-4658.2006.05130.x
26. Shivakumar, D., Williams, J., Wu, Y., Damm, W., Shelley, J., & Sherman, W. (2010, May 11). Prediction of Absolute Solvation Free Energies using Molecular Dynamics Free Energy Perturbation and the OPLS Force Field. J Chem Theory Comput, 6(5), 1509-1519. https://doi.org/10.1021/ct900587b
27. Tan, J., Verschueren, K. H., Anand, K., Shen, J., Yang, M., Xu, Y., Rao, Z., Bigalke, J., Heisen, B., Mesters, J. R., Chen, K., Shen, X., Jiang, H., & Hilgenfeld, R. (2005, Nov 18). pH-dependent conformational flexibility of the SARS-CoV main proteinase (M(pro)) dimer: molecular dynamics simulations and multiple X-ray structure analyses. J Mol Biol, 354(1), 25-40. https://doi.org/10.1016/j.jmb.2005.09.012
28. Wu, F., Zhao, S., Yu, B., Chen, Y. M., Wang, W., Song, Z. G., Hu, Y., Tao, Z. W., Tian, J. H., Pei, Y. Y., Yuan, M. L., Zhang, Y. L., Dai, F. H., Liu, Y., Wang, Q. M., Zheng, J. J., Xu, L., Holmes, E. C., & Zhang, Y. Z. (2020, Mar). A new coronavirus associated with human respiratory disease in China. Nature, 579(7798), 265-269. https://doi.org/10.1038/s41586-020-2008-3
29. Yang, H., Xie, W., Xue, X., Yang, K., Ma, J., Liang, W., Zhao, Q., Zhou, Z., Pei, D., Ziebuhr, J., Hilgenfeld, R., Yuen, K. Y., Wong, L., Gao, G., Chen, S., Chen, Z., Ma, D., Bartlam, M., & Rao, Z. (2005, Oct). Design of wide-spectrum inhibitors targeting coronavirus main proteases. PLoS Biol, 3(10), e324. https://doi.org/10.1371/journal.pbio.0030324
30. Yang, H., Yang, M., Ding, Y., Liu, Y., Lou, Z., Zhou, Z., Sun, L., Mo, L., Ye, S., Pang, H., Gao, G. F., Anand, K., Bartlam, M., Hilgenfeld, R., & Rao, Z. (2003, Nov 11). The crystal structures of severe acute respiratory syndrome virus main protease and its complex with an inhibitor. Proc Natl Acad Sci U S A, 100(23), 13190-13195. https://doi.org/10.1073/pnas.1835675100
31. Zhang, L., Lin, D., Sun, X., Curth, U., Drosten, C., Sauerhering, L., Becker, S., Rox, K., & Hilgenfeld, R. (2020, Mar 20). Crystal structure of SARS-CoV-2 main protease provides a basis for design of improved alpha-ketoamide inhibitors. Science. https://doi.org/10.1126/science.abb3405
32. Ziebuhr, J., Snijder, E. J., & Gorbalenya, A. E. (2000, Apr). Virus-encoded proteinases and proteolytic processing in the Nidovirales. J Gen Virol, 81(Pt 4), 853-879. https://doi.org/10.1099/0022-1317-81-4-853